



Enabling the use of lithium bis(trifluoromethanesulfonyl)imide as electrolyte salt for Li-ion batteries based on silicon anodes and $\text{Li}(\text{Ni}_{0.4}\text{Co}_{0.4}\text{Mn}_{0.2})\text{O}_2$ cathodes by salt additives

K. Asheim,^[a] I. F. Holsen,^[a] V. Renmann,^[a] M. V. Blanco,^[a] P. E. Vullum,^[b] N. P. Wagner,^[b] J.P. Mæhlen,^[c] and A. M. Svensson^{*[a]}

Lithium bis(trifluoromethanesulfonyl)imide (LiFSI) is a promising alternative salt for Li-ion batteries. Unlike the conventional LiPF_6 , it is not prone to HF formation, and thus resistant to moisture. However, for cell voltages relevant for high energy cathodes (> 4.2 V), the aluminium current collector will corrode in electrolytes based on this salt, and mitigation strategies are needed. Here, the use of Lithium tetrafluoroborate (LiBF_4) and Lithium difluoro(oxalato)borate (LiDFOB) salts as additives is investigated, in order to enable the use of LiFSI-based electrolytes. The performance of the electrolytes is evaluated separately for high content silicon anodes, $\text{Li}(\text{Ni}_{0.4}\text{Co}_{0.4}\text{Mn}_{0.2})\text{O}_2$ (NMC442) cathodes and the aluminium current collector by

electrochemical methods and post mortem analysis by SEM imaging and X-ray photoelectron spectroscopy (XPS). Electrolytes with LiDFOB as additive showed the best performance for all components, and were therefore selected for cycling in full cells, composed of silicon anodes and NMC442. Results show that LiFSI-based electrolytes with LiDFOB additive has an electrochemical performance similar to conventional electrolytes, and is thus a competitive, alternative electrolyte with a low fluorine content. Furthermore, it is verified that the good SEI forming properties of LiFSI based electrolytes known from cycling in half cells, is also preserved during cycling in full cells

Introduction

Li-ion batteries is one of the key enabling technologies for the transition to a renewable energy system.^[1,2] Due to the high energy density, Li-ion batteries is the technology of choice for all-electric vehicles. Still, improvements are needed with regards to energy density, safety and environmental impact. Currently, layered oxides like $\text{Li}(\text{Ni}_x\text{Co}_y\text{Mn}_z)\text{O}_2$ (NMC), with the highest possible content of Ni (x up to 0.8), is the dominating cathode material for high energy density Li-ion batteries. On the anode side, silicon is a good alternative to partially replace graphite, possessing 10 times the theoretical capacity (3600 mAh/g vs. 372 mAh/g). The difficulty with silicon is the large volume expansion experienced during lithiation (up to 300%).^[3,4] It is

therefore considered most realistic that silicon is added to graphite in silicon-graphite composite electrodes, in order to alleviate some of the strain and stresses associated with the large volume expansion of pure silicon anodes.

The strain on the electrode material as a consequence of the expansion of silicon electrodes results in numerous problems. One example is the integrity of passivation layer formed on the anode surface, i.e. the so-called solid electrolyte interphase (SEI). Cracks and damage to the SEI layer will lead to continued SEI formation,^[5] which again consumes lithium. Eventually the SEI layer might grow too thick and electrically insulate the active material. Thus, tailoring the electrolyte composition, in order to optimize the SEI properties, is crucial for implementation of electrodes with a high content of silicon. Current commercial Li-ion batteries have electrolytes composed of LiPF_6 as the main salt, in combination with carbonate solvents. Unfortunately LiPF_6 is susceptible to hydrolysis, and trace amounts of H_2O present in the cell will lead to formation of HF, which may damage both anode and cathode materials,^[6–10] for example by etching of the native oxide layer of silicon.^[10]

LiFSI does not hydrolyse, and is considered one of the most promising salts for replacing the conventional LiPF_6 salt.^[11] LiFSI has a higher Li^+ transport number than the LiPF_6 salt.^[12] Previous works have demonstrated benefits of LiFSI as electrolyte salt in combination with silicon anodes.^[10,13–15] Improved performance was demonstrated for anodes made from nano-silicon in half-cell configuration for LiFSI-based electrolytes in combination with carbonate solvents, attributed to the absence of HF in the electrolyte.^[10] Our previous work also verified the

[a] Dr. K. Asheim, I. F. Holsen, Dr. V. Renmann, Dr. M. V. Blanco,

Prof. A. M. Svensson

Department of Materials Science and Engineering,

NTNU, 7491 Trondheim, Norway

E-mail: annmari.svensson@ntnu.no

[b] P. E. Vullum, N. P. Wagner

SINTEF Industry, 7465 Trondheim, Norway

[c] J.P. Mæhlen

J.P. Mæhlen, Institute for Energy Technology,

2007 Kjeller, Norway

Supporting information for this article is available on the WWW under <https://doi.org/10.1002/batt.202300541>

© 2024 The Authors. *Batteries & Supercaps* published by Wiley-VCH GmbH. This is an open access article under the terms of the Creative Commons Attribution Non-Commercial License, which permits use, distribution and reproduction in any medium, provided the original work is properly cited and is not used for commercial purposes.

improved performance of LiFSI electrolytes compared with LiPF₆ for micron sized high silicon-content anodes, and a detailed post mortem study of the cycled electrodes revealed important differences in the SEI layers.^[14] The SEI found on electrodes cycled in LiFSI electrolytes appeared to be more homogeneous, stable, conductive and flexible, with a bilayer structure of an inner, predominantly inorganic layer, and an outer, predominantly organic layer, ensuring excellent passivation of the electrodes. The nature of the SEI layer relates to the rather high reduction potential of the LiFSI salt, around 1.7–1.9 V.^[10,14,16]

As carbonate solvents are volatile and flammable, and the salt LiPF₆ tends to decompose, conventional electrolytes are also associated with severe safety concerns when the cells are exposed to mechanical, thermal, or electrical abuse conditions.^[17] The presence of HF pose a threat to safety^[6,7] and complicates recycling and fire-extinguishing. LiFSI would improve safety significantly since this salt is much less prone to hydrolysis.^[18] Depending on the choice of the cathode material, LiFSI could potentially allow for higher dew point during production of battery cells, and thereby contribute to a significant reduction of the energy consumption during production of battery cells.

The main challenge with the LiFSI salt is occurrence of side reactions at potentials above 4 V,^[19,20] related to corrosion of the Al current collector on the cathode side or the stainless steel casing of the battery.^[21,22] While stainless steel can be avoided in Li-ion cells, replacing the aluminium current collector is challenging. The stability of aluminum current collectors is considered to rely on the presence of small amounts of HF in the electrolyte, for the formation of AlF₃ and Al-oxyfluorides.^[23–26] Passivation of the aluminum current collector may be facilitated by addition of hydrolyzing salts like LiPF₆ or LiBF₄.^[27] In fact, the salt LiBF₄ has proven to be even more efficient in suppressing corrosion of Al current collectors than LiPF₆.^[28] Alternatively, addition of lithium difluoro(oxalate)borate (LiDFOB) has also been shown to suppress Al corrosion.^[29–32] Park *et al.* found that the electrolyte based on LiFSI salt with addition of LiDFOB was less corrosive than electrolytes with additions of LiBF₄ and LiPF₆.^[30] The exact mechanism is however not agreed on. In the study of Park *et al.*,^[30] protective layers were identified on the surface of the Al current collector after addition of LiDFOB, containing Al–F species, as well as B–O/B–F components and Al₂O₃, while less Al–F species were found with LiBF₄ and LiPF₆ as additives. In the study of Yan *et al.*,^[31] on the other hand, the improved corrosion protection observed upon addition of LiDFOB was attributed to the formation of a polymeric film, possibly related to reaction with BF₂O[−] radicals.

There are also reports on positive effects of LiDFOB on the anode. Moderate improvements have been reported for thin film silicon anodes cycled with conventional LiPF₆ electrolytes with LiDFOB added.^[33] Here, electrolytes with LiDFOB added were found to generate surface films with high concentrations of oxalates and lithium fluorophosphates, but with reduced LiF content.^[33] Lee *et al.* studied conventional LiPF₆ electrolytes with 1 wt% LiDFOB added, in full cells with silicon-graphite composite anodes and cathodes made of a blend of LiCoO₂ and NMC622 (80:20 wt%), and demonstrated improved cycling

performance at 45°C.^[34] In this work, less lithium fluorophosphates were observed in the SEI after cycling in the LiDFOB containing electrolyte, which was taken as evidence for mitigation of LiPF₆ decomposition upon addition of LiDFOB. Other studies have focused on alternative solvents, or used LiDFOB as the only salt in the electrolyte. For fluorine-rich electrolyte solvents, based on dimethoxyethane (DME) and the 1,1,2,2-tetrafluoroethyl 2,2,3,3-tetrafluoropropyl ether (HFE), good performance of silicon electrodes was demonstrated for electrolytes based on LiFSI as salt, with addition of LiDFOB (1.2 M LiFSI and 0.05 M LiDFOB).^[35] Concentrated electrolytes with LiFSI and LiDFOB salts, and propylene carbonate (PC) as solvent, were shown to improve the performance of anodes fabricated from nano-silicon materials.^[15] This was attributed to the film-forming properties of LiDFOB, specifically the formation of Li(BF₂O)_n polymers. In a recent study where trimethyl phosphate (TMP) was used as a solvent in combination with micro-sized silicon electrodes and LiNi_{0.5}Mn_{1.5}O₄ (LNMO) cathodes, better cycling stability was demonstrated with the LiDFOB salt compared to LiPF₆.^[36] For porous germanium anodes, electrolytes made from carbonate solvents and LiDFOB as the only salt showed improved performance compared to LiPF₆, attributed to the SEI formed in this electrolyte, consisting of amorphous inorganic particles embedded in the organic matrix.^[37] Electrolytes with LiDFOB as the only salt have also been shown to work well with cells with a NMC622 cathode and metallic lithium anode.^[38] For this system, reasonable performance was obtained with 1,2 ethylene sulfite solvent (ES), while stable performance could not be demonstrated for carbonate solvents (due to poor quality of the SEI and cathode electrolyte interphase (CEI) layers). To our knowledge there are no reports on the SEI forming properties of LiDFOB on silicon anodes in combination with LiFSI salts and conventional carbonate solvents. The reduction potential of LiDFOB has been shown to lie around 1.5 V,^[34] i.e. below the reduction potential of LiFSI (1.7–1.8 V^[39]), but above the reduction potentials of EC, FEC and LiPF₆,^[40] which can affect the SEI formation.

Studies of full cells with LiFSI salts are limited in the open literature. Recently, good performance of NMC111-Si/graphite cells was achieved with the concentrated LiFSI:EC 1:2 electrolyte, both at the room temperature and elevated temperature (55 °C).^[41] One previous work has demonstrated cycling of full cells based on silicon-graphite composite anodes (with 15 wt% of silicon) and NMC cathodes, and electrolytes based on LiFSI salts only. The cycling performance was similar to the performance obtained with LiPF₆-based electrolytes, provided that fluoroethylene carbonate (FEC) was also added.^[42] However, the upper cut-off voltage was set to 4.1 V to avoid corrosion of the Al current collector. Cao *et al.* have demonstrated significant improvement of silicon graphite electrodes for solvent mixtures of dimethoxyethane (DME), FEC and 1,1,2,2-tetrafluoroethyl 2,2,3,3-tetrafluoropropyl ether (HFE), combined with salt mixtures of 1.2 M LiFSI and 0.05 M LiDFOB.^[35] Also in this work, the upper cut-off voltage was 4.1 V. From studies of full cells utilizing silicon-graphite composite as anodes, it is generally agreed that the relatively rapid loss of capacity observed is related to the loss of active lithium in the cells, as lithium is

consumed in the SEI forming reactions.^[43,44] Furthermore, the SEI formation may be altered by the lack of lithium in full cells, eventually forming lithium-free organic degradation products, as observed by Dupré *et al.*,^[45] which leads to differences in the SEI formed in full cells compared to half cells.

The main purpose of this work is to demonstrate the possibility of reducing the fluorine content in Li-ion full cells composed of silicon anodes (60 wt% of micron sized, low cost battery grade silicon), and NMC442 cathodes. The focus is on electrolytes with 1 M concentration of LiFSI and conventional carbonate solvents. In order to mitigate the corrosion of the aluminium current collector, two additives are compared, namely LiBF₄ and LiDFOB. The effect of addition of 0.2 M of these additives is investigated with silicon-rich anodes, to obtain information on the SEI forming properties, and NMC442 cathodes in half cells, up to 4.5 V as well as bare aluminium current collectors. NMC442 cathodes together with the silicon-rich anodes are then cycled in full cells together with the most promising electrolytes. After cycling in half cells and full cell, silicon anodes, as well as the aluminium current collector, are subject to post mortem characterization by SEM, cross section analysis, TEM imaging and element mapping (for the silicon-graphite electrodes), and surface analysis by XPS. In addition to providing useful information on the surface layers formed, the analysis could verify whether differences between the SEI formed in half cells in the LiFSI and LiPF₆-based electrolytes are still observed after cycling in full cells.

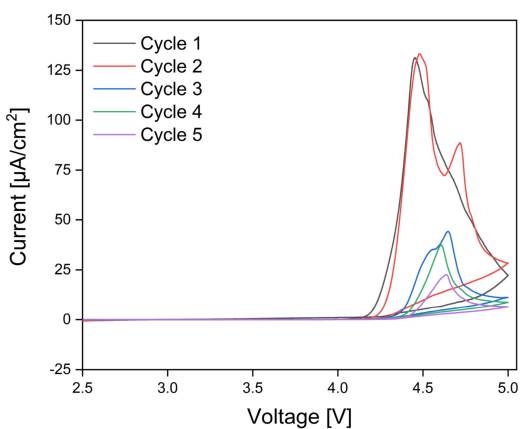
Results and Discussion

Corrosion resistance of the aluminium current collector

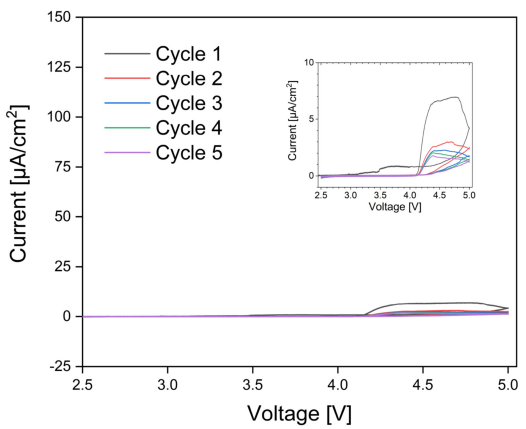
The effect of additions of the salt additives LiDFOB and LiBF₄ on the corrosion resistance of the aluminium current collector was investigated by cyclic voltammetry in half-cell configuration at a slow scan rate (0.1 mV/s). The results are shown in Figure 1. A high oxidation current, as expected, is observed for the 1 M LiFSI electrolyte, with an onset potential of around 4.2 V. It should be noted, however, that the oxidation currents decrease significantly after the second cycle. Corrosion is mitigated upon addition of LiDFOB and LiBF₄, and peak currents are reduced by a factor of around 20 for LiBF₄, and almost 2 orders of magnitude for LiDFOB.

A collection of SEM images of the aluminium surface after the CV scans is shown in the Supporting Information, Figure S1, for all electrolytes. In brief, the surface of the aluminium after conducting the CV-scans in the LiFSI electrolyte exhibit several large pits, in addition to layers of deposits. A thin deposit appear to cover more or less the entire surface, while there are also regions of thick deposits, typically located in next to large pits. Small deposits are found also on the surface of aluminium cycled with LiDFOB and LiBF₄ additives, but the amount significantly smaller than for the LiFSI electrolyte.

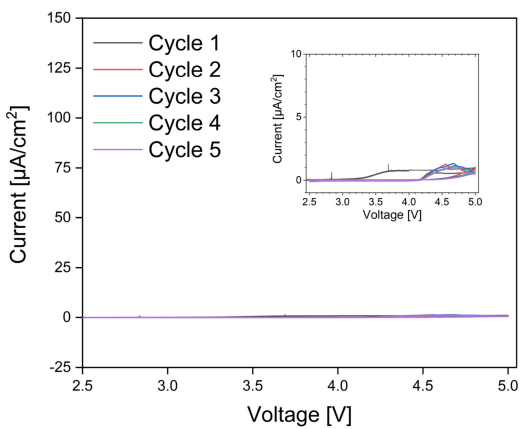
In order to obtain more information on the chemical nature of the surface after cycling in the various electrolytes, XPS spectra were recorded. Figure 2 shows the Al 2p feature of the



a)



b)



c)

Figure 1. Cyclic voltammograms of aluminium current collectors in a) 1 M LiFSI electrolyte b) 1 M LiFSI + 0.2 M LiBF₄ electrolyte c) 1 M LiFSI + 0.2 M LiDFOB electrolyte.

aluminium electrodes after one CV cycle in the different electrolytes, together with a pristine Al sample. As the binding energies of Al–F and Al–O features are close, these peaks could not be easily deconvoluted. Still, the high energy peak of the

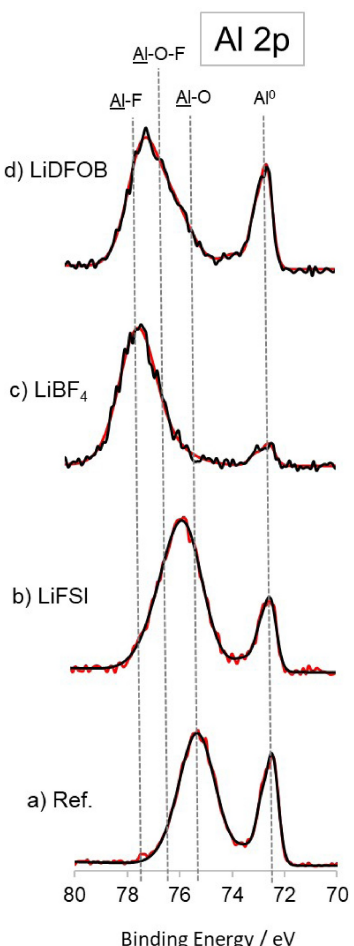


Figure 2. Al2p spectra of a) fresh aluminium surface and after 1 CV scan for b) 1 M LiFSI electrolyte c) 1 M LiFSI + 0.2 M LiBF₄ electrolyte d) 1 M LiFSI + 0.2 M LiDFOB electrolyte.

LiBF₄ containing electrolyte is shifted more towards the Al–F binding energy, compared to the electrolyte with only FSI, which is more shifted towards Al–O–F. The LiDFOB containing electrolyte is somewhere between these. Corrosion protection of the Al current collector has previously been proposed to be related to formation of an AlF₃ layer on top of the Al₂O₃ layer,^[25,26,46] alternatively referred to as a protective Al_xO_yF_z layer.^[24]

The element analysis from the survey scans, the F 1s spectra, as well as the C 1s spectra are provided in the Supporting Information, section S2 and Figure S2. From the element analysis it is observed that the total content of fluorine is highest for the LiBF₄ containing electrolyte. The F 1s spectra confirm that the peak observed in LiBF₄ is more shifted towards the Al–F binding energy, whereas for the LiDFOB containing electrolyte, the F 1s spectrum is more shifted towards LiF. Also, for this electrolyte, the C 1s spectra clearly indicate a higher fraction of organic products found on the surface of the aluminium foil. In a previous study of Al current collectors in combination with an electrolyte of 1 M LiFSI and 2 wt% LiDFOB in EC:EMC solvent, the surface was also found to be rich in organic compounds.^[31] This was proposed to be related to the

formation of BF₂O[−] upon oxidative decomposition of LiDFOB, causing ring-opening and polymerisation of the EC, providing a surface layer protective against Al corrosion and LiFSI decomposition. The high content of Al–F features in the LiBF₄ containing electrolyte is in agreement with results obtained by Mun *et al.*,^[47] upon cycling of Al current collectors in an electrolyte of LiBF₄ and TFSI based ionic liquid. Park *et al.*^[30] also observed significant corrosion inhibition of the Al current collector upon addition of LiDFOB and LiBF₄ to an LiFSI electrolyte, but attributed the corrosion protection to formation of a thick Al₂O₃ layer, possibly with B–O/B–F species on top in the case of LiBF₄, while the protective layer formed in the LiDFOB containing electrolyte was found to contain Al–F, B–F and B–O species.

Electrochemical Characterization of NMC Cathodes

A comparison of the discharge capacities of the NMC442 electrodes in half-cell configuration with LiFSI-based electrolytes, with 0.2 M LiDFOB or LiBF₄ as additives, is shown in Figure 3. All the cells cycling in the voltage range 3.0 – 4.2 show a very stable performance, with discharge capacity of 120 mAh/g and coulombic efficiency close to 100% throughout the cycling. Cycling in the voltage range 3.0–4.5 eV results in stable cycling with capacity around 150 mAh/g, with the LiDFOB additive giving a slightly higher capacity, and coulombic efficiency close to 100% for the cells with additives. The cell with pure LiFSI electrolyte shows a declining capacity, from 140 to 90 mAh/g over 50 cycles, and a coulombic efficiency around 98%.

The results shown in Figure 3 are consistent with the results obtained for the aluminium current collector. The LiFSI-based electrolyte appear to have an onset potential for oxidation currents of around 4.2 V. Thus, for an upper cut-off voltage of 4.5 V, corrosion of the aluminium current collector is expected for the LiFSI electrolyte. It should also be noted, that for full cells with silicon anodes, the potential of both electrodes is likely to increase during cycling. In our previous work, a potential increase of 0.3 V was observed for cells with a silicon anode and a NCA cathode over cycles,^[48] thus illustrating the need for performing half cell experiments at relatively high cut-off values.

LiDFOB is a well-known film-forming additive for both anode and cathode, as the HUMO and LUMO levels are within the levels of conventional electrolyte solvents, like EC, DMC and EMC,^[49] implying that LiDFOB will oxidize prior to the solvents. An oxidation potential of 4.15–4.23 V has been reported.^[49,50] The formation protective films on the surface of spinel LiMn₂O₄,^[51] as well as Li_{1.18}Ni_{0.15}Mn_{0.52}Co_{0.15}O₂ cathodes^[52] have been demonstrated in the presence of electrolytes containing only the LiDFOB salt. LiDFOB is, however, more commonly applied as an electrolyte additive^[49,50,52,53] to LiPF₆ based electrolytes in carbonate solvents, to minimize the resistance associated with the films formed,^[52] as has also been demonstrated for Li_{1.2}Ni_{0.15}Mn_{0.55}Co_{0.1}O₂ cathodes in full cells.^[53] After long term cycling in full cells at a cut-off voltage of 4.6 V, the rise in

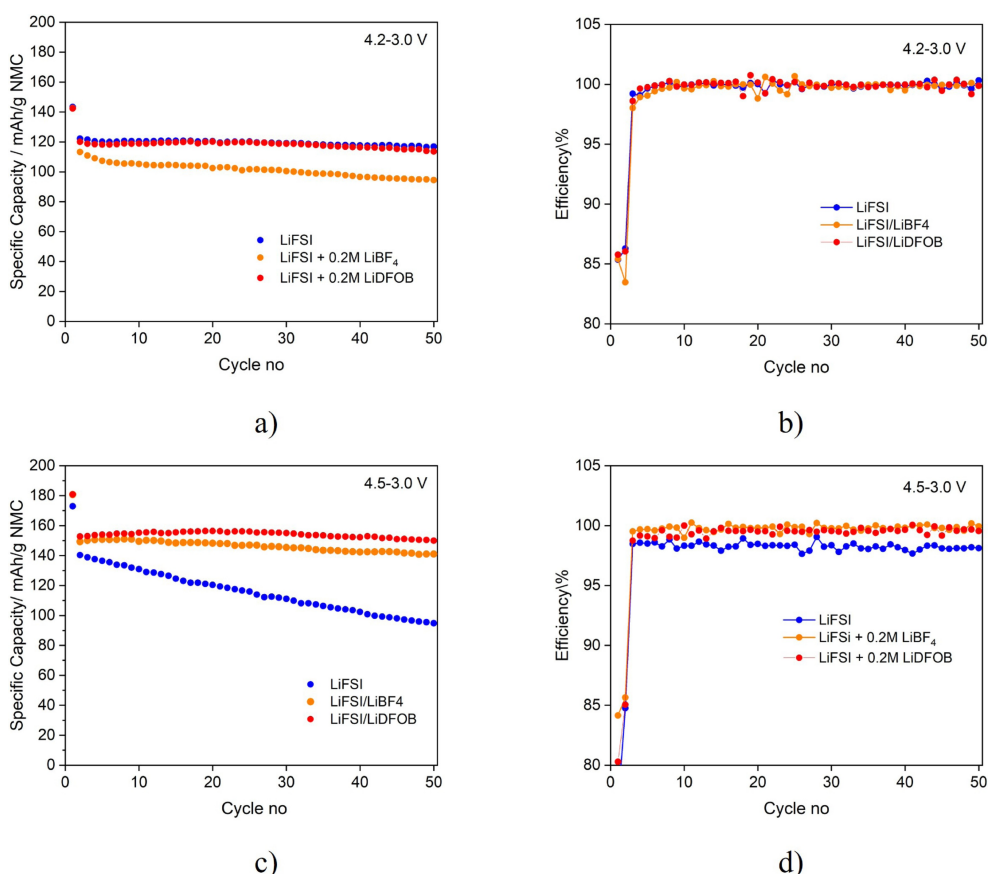


Figure 3. Performance of NMC half-cells in LiFSI electrolyte with LiDFOB and LiBF₄ as additives. a) Discharge capacity versus cycle number, with upper cut-off of 4.2 V. b) Coulombic efficiency versus cycle number, with upper cut-off of 4.2 V. c) Discharge capacity versus cycle number, with upper cut-off of 4.5 V. d) Coulombic efficiency versus cycle number, with upper cut-off of 4.5 V.

impedance for this cathode was significantly higher for the conventional LiPF₆ electrolyte than for the electrolyte with LiDFOB additive. The improved stability was attributed to formation of a passivation layer, resulting from decomposition of carbonates by radicals formed by the oxidative decomposition of LiDFOB, also preventing the transition metal dissolution.^[53] Gao *et al.*^[50] also demonstrated that addition of LiDFOB could improve the cycling performance of NMC622 for voltages up to 4.6 V, by forming protective films to help mitigate solvent decomposition. No significant increase in the impedance of the cathode was observed. Similar findings were reported also for NMC811 upon addition of LiDFOB to a LiPF₆ electrolyte in EC:EMC solvent.^[49] LiDFOB has also been studied as an additive to LiFSI-based electrolytes. For NMC442 cathodes in combination with thin, metallic lithium anodes, and an electrolytes based on LiFSI with LiDFOB as additive,^[54] the electrochemical performance (cycling performance and impedance) was shown to be similar for LiFSI/LiDFOB electrolyte and the LiPF₆-based electrolyte. Thus, in spite of differences in the chemical composition of the CEI (presence of boron, for example), these do not affect significantly the resistance of the layers formed on the electrodes. It seems therefore reasonable to assume that the formation of a passivation film with LiDFOB

as additive does not appear to cause any additional polarization of the cathode, regardless of the main salt (LiPF₆ or LiFSI).

Electrochemical Performance of Silicon Anodes

Initially, the effect of addition of LiDFOB and LiBF₄ to the electrolyte on the performance of silicon electrodes was investigated. Half-cells were assembled with and without LiDFOB and LiBF₄, and galvanostatically cycled. The results are presented in Figure 4, showing the average specific capacity of 3 cells, and coulombic efficiency versus cycle number.

The cells exhibit an initial capacity of 2500, 2776 and 2719 mAh/g in the formation cycle for 1 M LiFSI, 1 M LiFSI + 0.2 M LiBF₄, 1 M LiFSI + 0.2 M LiDFOB, respectively. After 100 cycles, the capacities have dropped to 1590, 1546 and 1645 mAh/g, respectively. The capacity drops steadily for the electrolyte with LiBF₄ added, but goes through a maximum for the LiFSI and LiFSI + 0.2 M LiDFOB electrolytes (at cycle 6 and 17). The coulombic efficiencies have very similar initial value of 80.5%, 81.5% and 80.3% for LiFSI, 0.2 M LiBF₄ and 0.2 M LiDFOB, respectively. After the 4th cycle, the CE varies somewhat between 98.8% and 99.5% for all electrolytes.

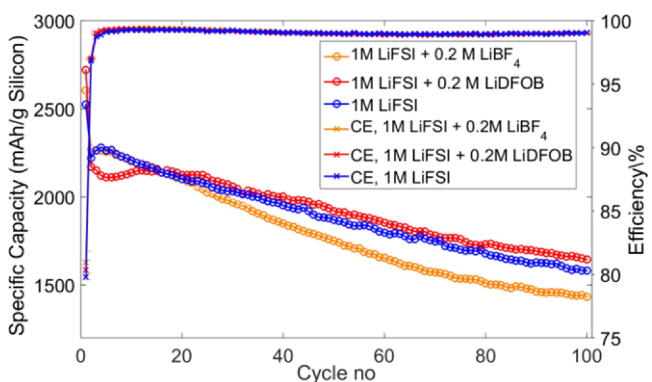


Figure 4. Averaged performance of Si half-cells in LiFSI electrolyte with 0.2 M LiBF₄ or 0.2 M LiDFOB as additives. Specific capacity versus cycle number and (left axis) coulombic efficiency versus cycle number (right axis).

From Figure 4 the addition of LiDFOB appears actually to slightly improve the performance of Si electrodes compared to addition of LiBF₄, or the pure LiFSI electrolyte. The capacity retention after 100 cycles was 74%, 64% and 71% for the electrolytes with addition of 0.2 M LiDFOB, 0.2 M LiBF₄ and 1 M LiFSI, respectively. Addition of small amounts of LiDFOB to LiPF₆ based electrolytes has been suggested to improve the performance of silicon-graphite composite anodes,^[33] as well as for NMC/Silicon-graphite full cells.^[34] For fluorine-rich electrolyte solvents, based on HFE, good performance of silicon electrodes was demonstrated for electrolytes based on LiFSI as salt, with addition of LiDFOB (1.2 M LiFSI and 0.05 M LiDFOB).^[35] Electrolytes based on pure LiBF₄ has been shown to result in inferior performance of binder-free graphite electrodes,^[40] while addition of 10 wt% LiBF₄ to the LiPF₆ electrolyte improved the performance.^[55]

The LiDFOB salt has been shown to reduce at potentials around 1.6–1.8 V,^[15,34,38,40,56] i.e. slightly below the reduction potentials reported for LiFSI, in the range 1.8–2.2 V.^[57,58] As discussed in previous works,^[57] the reduction potential of LiFSI is strongly depending on the solvent. For a similar carbonate solvent mixture as the one used here, a reduction peak around 1.8 V has been reported.^[59] Thus, for electrolytes based on either 1 M LiFSI, or 1 M LiFSI+0.2 M LiDFOB, the initial SEI formation implies the reduction of salts, while all solvent components have lower reduction potential, and will contribute to the formation of organic SEI components on the outer surface of the SEI. It should also be noted that there is no significant difference between the polarisation observed for the 1 M LiFSI and the 1 M LiFSI+0.2 M LiDFOB electrolytes, while a slightly

higher polarization is seen for LiBF₄ (see Figure S3 in Supporting Information).

Post mortem characterisation of the cycled Si electrodes by XPS

Table 1 shows the atomic percentages of the elements present in the SEI layer of anodes cycled with LiFSI, LiFSI+0.2 M LiBF₄ and LiFSI+0.2 M LiDFOB electrolytes after 100 cycles. For all the electrolytes, the amount of detected silicon and sodium (from the Na-CMC binder) decrease significantly after 100 cycles due to the formation of a SEI layer on the anode surface. The highest amount of Si is detected on the electrode cycled with the LiFSI/LiBF₄ electrolyte, indicating the formation of a thinner SEI layer with this electrolyte. The SEI on the electrode cycled in LiFSI/LiDFOB electrolyte appears to be dominated by organic compounds, due to the presence of more carbon and less fluorine, lithium and sulfur in this layer. Previous works have also suggested the presence of lithium oxalate and oligomeric borates in the SEI, which are carbon rich species, upon addition of LiDFOB.^[15,56,60–62] The SEI layer formed in the presence of LiBF₄ appears to be dominated by inorganic species, such as LiF. Similar results were obtained in the work of Xu *et al.*,^[63] where a range of salts were compared in combination with binder-free graphite electrodes. In this work, the SEI formed in LiBF₄ resulted in higher fractions of LiF on the surface compared to other salts (including LiFSI, LiDFOB and LiPF₆). Additionally, borate is present in the SEI layers formed in LiBF₄ and LiDFOB containing electrolytes. The amount is more than doubled for the LiBF₄ additive compared to the LiDFOB additive. It has been suggested that the LiBF₄ salt decompose more easily to form borated species such as alkyl borates, lithium borates and lithium fluoroborates in the SEI layer,^[61] while the LiDFOB salt is more stable.

Figure 5 shows the core level peaks of C 1s, O 1s and F 1s for the anodes after 100 cycles. The C 1s peaks can be assigned to C–C and C–H bonds at 285 eV, C–O at 286.5 eV, overlapping C=O and O=C=O peaks around 288 eV and Li₂CO₃ around 289–290 eV.^[10] For the LiDFOB containing electrolyte, a rather broad peak between 288 and 290 eV most is most likely an overlap of C=O, O=C=O and Li₂CO₃ features. For the LiBF₄ and LiDFOB additives, the peak at 291 eV is assigned to a –CHF–OCO₂–type reduction product from FEC.^[64–67] For LiFSI and the LiDFOB additive, a peak is observed at 282.8 eV and 282.4 eV, respectively, corresponding to lithiated carbon.^[16,68]

Table 1. Elemental composition in at.% of Si electrode surfaces after 100 cycles in 1 M LiFSI, 1 M LiFSI+0.2 M LiDFOB or 1 M LiFSI+0.2 M LiBF₄ electrolyte, acquired from survey spectra after XPS measurement.

Element	Si	Na	C	O	F	Li	B	N	S
Fresh Si anode	8.2	0.7	73.9	17	–	–	–	–	–
1 M LiFSI	0.5	0.1	24.2	25.6	13.3	24.4	–	3.4	8.5
LiFSI+LiBF ₄	1.1	0.4	16.3	24.3	17.1	30.2	4.6	1.9	4.2
LiFSI+LiDFOB	0.2	0.3	37.5	25.2	9.2	21.6	1.9	1.4	2.7

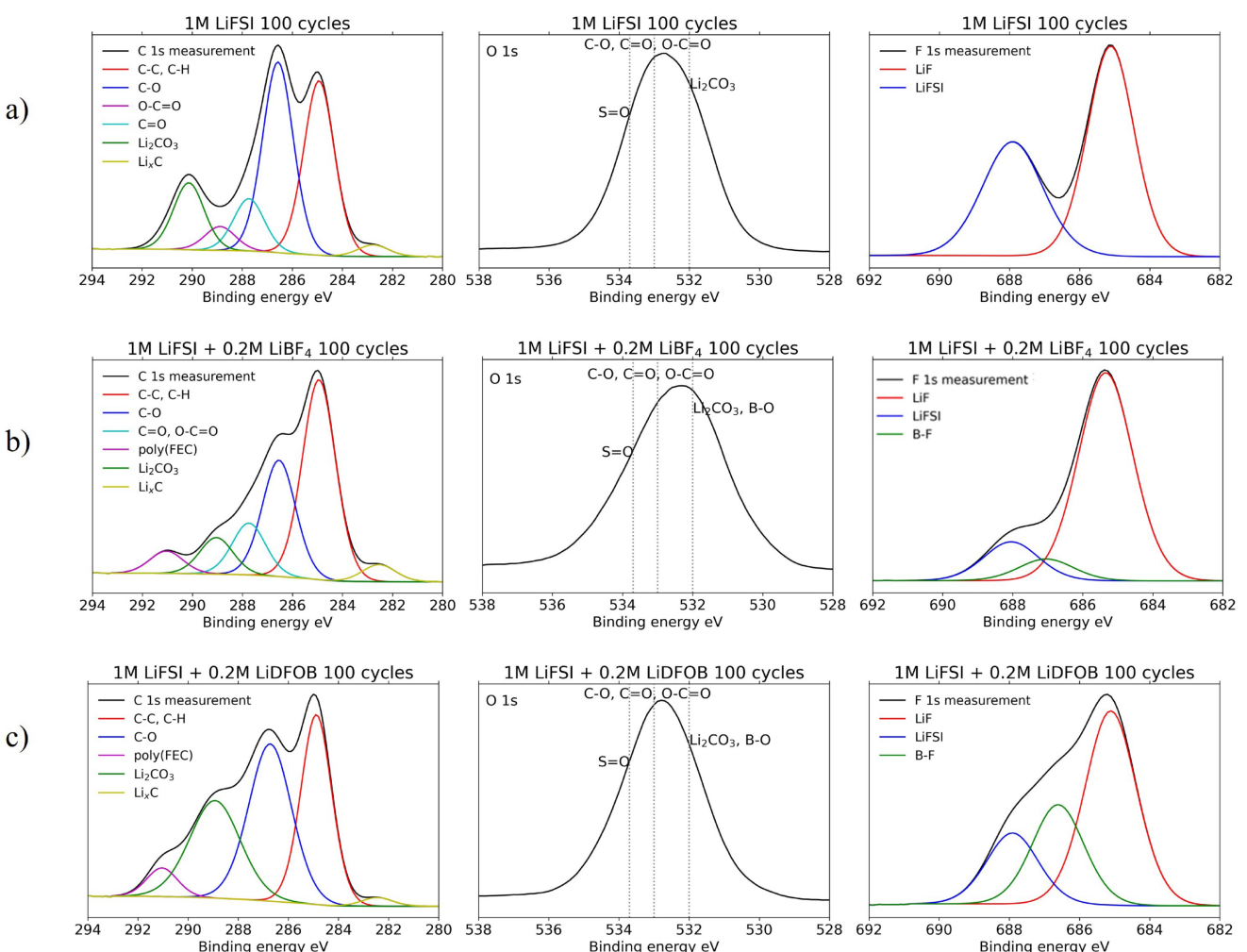


Figure 5. C1s, O1s and F1s spectra for Si electrodes after 100 cycles in a) 1 M LiFSI electrolyte b) 1 M LiFSI + 0.2 M LiBF₄ electrolyte c) 1 M LiFSI + 0.2 M LiDFOB electrolyte.

The O 1s peaks shown in Figure 5 correspond to organic components, such as C–O, C=O and O–C=O, at 533 eV, Li₂CO₃ at 532 eV and a S=O feature at 533.7 eV.^[10,69] The organic species in the O 1s spectra are often overlapping in the region of 531–534 eV,^[66] and could therefore not be resolved. For the LiBF₄ and LiDFOB additive, an additional peak was observed at 532 eV, attributed to B–O feature, likely to be decomposition products of the borated salts such as alkyl borates (B(OR)₃) (R = alkyl group), lithium borates (Li_xBO_y), lithium fluoroborates (Li_xBO_yF_z) and cross-linked oligomeric borates (only observed for LiDFOB).^[15,61] The O 1s spectra also indicate that the SEI formed in the LiBF₄ containing electrolyte has a higher fraction of inorganic species, than the LiDFOB containing electrolyte, as discussed above.

The F 1s peaks shown in Figure 5 are dominated by the features of LiF at 685 eV and the S–F bond of LiFSI at 688 eV. In addition, a peak at 687 eV is seen for the LiBF₄ containing electrolyte, and at 686.6 eV for the LiDFOB containing electrolyte, attributed to a B–F feature.

The Li 1s and B 1s peaks are shown in the Supporting Information, Figure S4. The peaks of the Li 1s spectra are

attributed to a LiF feature at 56 eV and Li₂CO₃ at 55.5 eV, which could also contain lithium bound to organic components. The SEI from the LiBF₄ containing electrolyte is dominated by the LiF peak, both in the F 1s spectra and the Li 1s spectra, in accordance with the high amounts of Li and F in the survey scan, confirming the high amount of LiF in the SEI layer in the presence of LiBF₄ salt. The Li 1s signals for LiFSI and LiDFOB electrolytes are dominated by the Li₂CO₃ peak. The B 1s spectra are deconvoluted into B–F and B–O features (Figure S4d) and e)). For the LiBF₄ containing electrolyte, the B–O feature is dominating, which has previously also been observed,^[70] and must be related to reactions involving the solvent or SEI compounds.

The LiDFOB electrolyte appear to have a slightly higher share of organic components than the LiFSI. Chemical reduction of LiDFOB has previously been found to result in decomposition products like lithium oxalate, Li₂CO₃, and crosslinked oligoborates.^[71] DFT calculations indicate that the B–O bond of the LiDFOB salt has a negative bond strength,^[54] and will therefore decompose into an oxalate anion and BF₂. Thus, the B–F bonds are relatively stable in LiDFOB, which might provide

an explanation for the low amount of LiF. In the work of Chang *et al.*, nano-silicon electrodes were cycled in dual salt electrolytes of LiFSI and LiDFOB (70:30), with PC as the solvent.^[15] Based on the higher fraction of B–F with respect to B–O features in the XPS spectra, the SEI was suggested to be composed of Li(BF₂)On-polymer and lithium oxalate, associated with ring opening reduction of LiDFOB and PC. The improved electrochemical performance observed for the mixed electrolyte was attributed to the presence of Li(BF₂)On polymers, leading to a flexible and passivating SEI. These results are consistent with our results, even if the exact nature of organic compounds are hard to prove by XPS only.

Overall, the addition of LiBF₄ leads to formation of an SEI layer which is thin, and rich in salt reduction products like LiF and Li₂BF_y, similar to previously reported results for SEI layers for electrolytes with LiBF₄ as the only salt.^[40,60,72] Upon addition of LiDFOB, however, the SEI is rich in organic compounds, there are less salt reduction products, and the SEI appears more similar to the SEI formed in the pure LiFSI electrolyte. This is further supported by the XPS spectra, where LiFSI and LiDFOB electrolytes clearly show an outer SEI enriched in organic components. Thus, addition of LiBF₄ disrupts the good SEI forming properties known for LiFSI-based electrolytes,^[10,14] related to the HF formation in this electrolyte, while the SEI film-forming properties shown for LiDFOB salt for other electrolyte systems^[15,49,73] appear also here to provide a good quality SEI.

Full-cell configuration

Given the excellent performance upon of the LiDFOB containing electrolyte compared to LiBF₄, with respect to cycling of silicon anodes, NMC cathodes as well as the Al current collector corrosion, electrolytes with 1 M LiFSI and 1 M LiFSI + 0.2 M LiDFOB, were selected for cycling in full cells, with 1 M LiFSI and 1 M LiPF₆ in the same carbonate solvent mixture as references.

In Figure 6a) the average specific capacity w.r.t. NMC versus cycle number for all electrolytes is presented, and in Figure 6b) the coulombic efficiency versus cycle number. The initial capacities for the cells were 128, 132 and 138 mAh/g(NMC) for 1 M LiFSI, 1 M LiPF₆ and 1 M LiFSI + 0.2 M LiDFOB, respectively. The capacity retention after 200 cycles was 28% in 1 M LiFSI, 25.5% in 1 M LiPF₆ and 28% in 1 M LiFSI + 0.2 M LiDFOB. The coulombic efficiencies are initially highest, but noisy, for the LiPF₆ and LiFSI + 0.2 M LiDFOB electrolytes, which is typically attributed to release of trapped lithium from the silicon anode from previous cycles. After approximately 40 cycles, the coulombic efficiency drops to 99% for the LiPF₆ electrolyte, while it remains slightly higher for both LiFSI based electrolytes. Similar performance for LiPF₆ and LiFSI-based electrolytes in carbonate solvent were also demonstrated in NMC-silicon/graphite full cells, provided that FEC was used as additive.^[42] It should be noted that the upper cut-off voltage in this work was limited to 4.1 V.

The poor capacity retention is to be expected, given the high utilization of the silicon electrodes in this case (more than

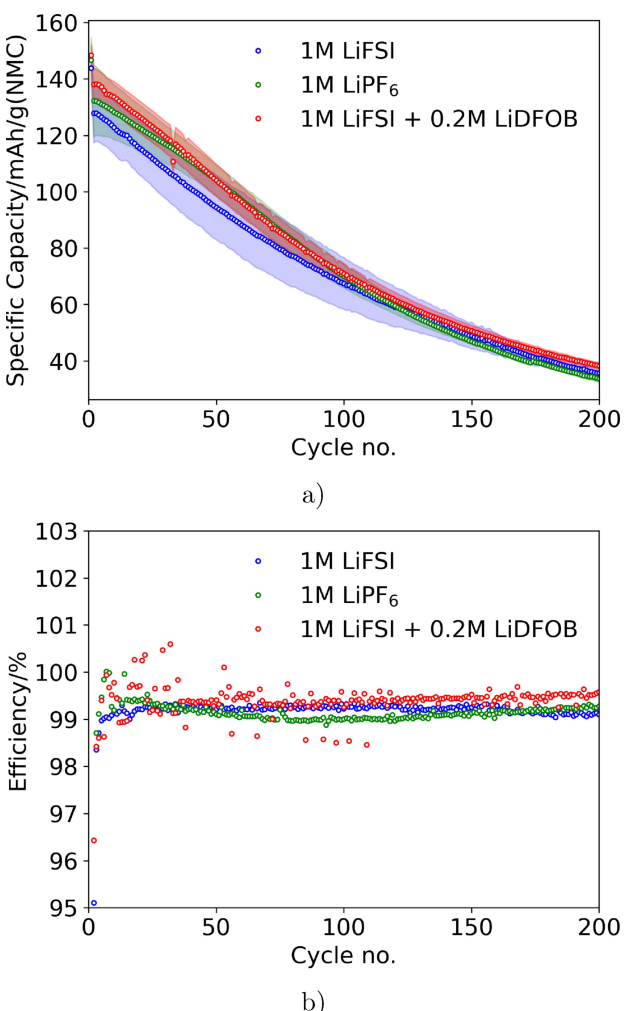


Figure 6. Averaged performance of full-cells with the different electrolytes. a) Specific capacity versus cycle number. The standard deviation of the data in a is included as the light colored areas above and below the data points. b) Coulombic efficiency as a function of cycle number.

2000 mAh/g). Beattie *et al.*^[43] obtained a capacity retention just below 50% after 200 cycles for high-loading electrodes made from 70 wt% of a similar silicon, with a utilization of 1600 mAh/g(Si). In our previous work,^[48] a capacity retention of 80% after 150 cycles was obtained in full cells for electrodes of similar composition, where the anodes were designed to deliver 1200 mAh/g(Si) for the set n/p ratio. The unusually high utilization used for this work is expected to exaggerate potential differences between the electrolytes during long-term cycling.

From the differential capacity plots in Figure 7, it is seen that the charging peak (plateau) is shifted to higher potentials in a similar manner for all electrolytes. The corresponding voltage curves are provided in Figure S5 in Supporting Information. However, while the discharge plateau is shifted towards similar values for the LiPF₆ and the 1 M LiFSI + 0.2 M LiDFOB electrolyte, implying that the polarisation increase from around 0.2 V in the second cycle to around 0.25 V in cycle no. 200, the shift is way higher for the 1 M LiFSI electrolyte, resulting in a polarisation at cycle 200 of around 0.4 V. In other

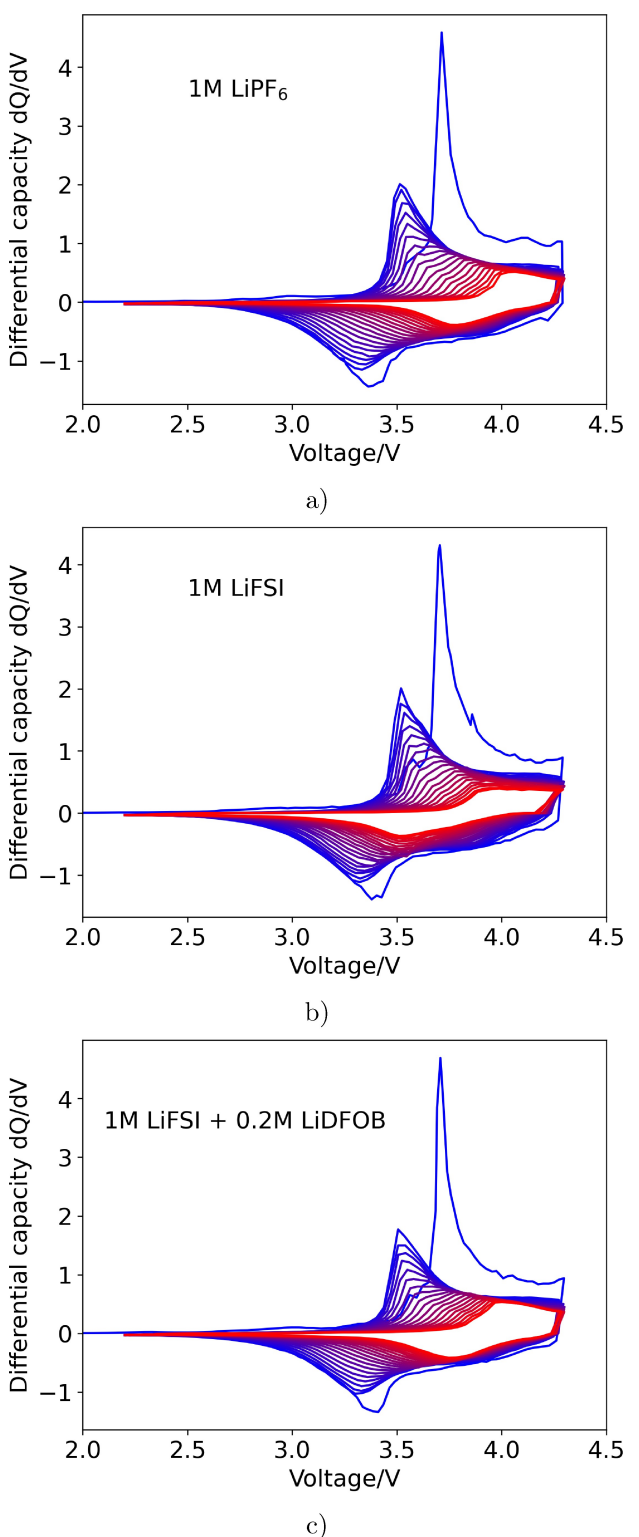


Figure 7. Differential capacity plots derived from voltage profiles of full cells, for a) 1 M LiPF₆, b) 1 M LiFSI and c) 1 M LiFSI + 0.2 M LiDFOB. Every 10th cycle is plotted with color gradient from blue (first cycle) to red (200th cycle).

works, the potential at both electrodes is found to increase during cycling of similar electrodes in full cells with a 3-electrode configuration,^[43,48] implying that cathode voltages

in the range 4.4–4.6 eV with respect to Li/Li⁺ are reached. In view of the degradation of the cathode at the highest voltage, shown in Figure 3, it is therefore not unexpected that an additional polarization arise on the NMC electrodes in the LiFSI electrolyte during cycling. The additional polarization is also evident by comparison of the capacities obtained during the potentiostatic hold step. At charge, the step corresponds to a constant capacity of 2–3 mAh/g(NMC) for all cycles with 1 M LiPF₆ and 1 M LiFSI + 0.2 M LiDFOB. Initially, the step corresponds to 3 mAh/g(NMC) for LiFSI, increasing to 6 mAh/g(NMC) after 200 cycles, indicating more severe kinetic limitations over time for this electrolyte. However, the electrolyte with only LiFSI results in better performance than expected given reports on issues with Al corrosion when using this salt.^[18,74] It should be noted that in these studies, coin cells were used, and it was debated whether Al corrosion was due to the LiFSI salt, proven to be incompatible with steel^[75] or Cl⁻ contamination. Overall, the addition of LiDFOB to the LiFSI electrolyte appears to improve the performance of these NMC/silicon full-cells.

The capacity fade observed in Figure 6 is related to the loss of the lithium inventory, as has already been suggested in other works.^[42–44] The difference in cycling performance is furthermore attributed to loss of capacity for the NMC cathode, observed from half cell experiments when cycled in LiFSI at potentials higher than 4.3 V for LiFSI electrolytes, while the cycling is stable upon addition of 0.2 M LiDFOB. Regarding the poor performance of the NMC at higher potentials, corrosion of the aluminum current collector is considered to be the most likely explanation. In the work of Trask *et al.*,^[42] the performance degradation of full cells with NMC and silicon-graphite composite electrodes in LiFSI electrolyte was attributed entirely to the anode. In this work the silicon-graphite composite contained only 15 wt% of silicon, and the upper cut-off voltage was 4.1 V, so possible shifts in electrode potentials are also expected to be lower. From Figures 6 and 7, there is no significant difference between the LiPF₆ and the 0.2 M LiDFOB electrolyte, as even the differential capacity curves evolves in an identical manner for the two electrolytes, with similar reductions and shifts of both anodic and cathodic peaks.

Post mortem characterisation of Si electrodes cycled in full cells

In this section, results from extensive post mortem characterisation of the silicon electrodes cycled in full cells, by SEM, FIB-SEM, TEM and XPS are presented. A comparison is made to our previous extensive study with similar electrodes, in combination with LiFSI and LiPF₆ electrolytes in half cells, to identify potential differences between the SEI formed in full cells and half cells.^[14] The main aim of the post mortem characterization is to verify that the beneficial structure of the SEI formed in LiFSI containing electrolytes, with an inner layer of inorganic compound, and an outer layer of primarily organic, ensuring the flexibility of the SEI, is present also in full cells.

FIB-SEM analysis for evaluation of electrode morphology

The micrographs of electrode cross sections, Figures 8a) and 8b), clearly shows that after 10 cycles, the Si electrode cycled in LiPF₆ is subject to more roughening of the particle surface and a more severe expansion of the electrodes. As the capacities are rather similar, this indicates a less uniform lithiation of the silicon, most likely related to a less uniform SEI on the particle surface. SEM micrographs of the surfaces of the electrodes are shown in the Supporting Information, Figure S7. For comparison, Figure S6a) in the Supporting Information, shows the examples of a SEM micrograph of the surface of the pristine silicon electrode, and the cross section of a pristine electrode is shown in Figure S6b).

TEM analysis of Si particle morphology

Figure 9 show high angle annular dark field scanning transmission electron microscopy images of silicon particles after 10 cycles in either 1 M LiFSI, Figure 9a), or 1 M LiPF₆, Figure 9b), electrolyte. The corresponding image of the pristine silicon is shown in Figure S6c). From the micrographs, a large difference in Si particle morphology after 10 cycles is seen for the two electrolytes. Just like in the cross section micrographs above, the Si particle in Figure 9b), cycled in the LiPF₆ electrolyte, clearly has been less uniformly lithiated than the largest Si particle in Figure 9a), where LiFSI was the electrolyte salt. For the Si particle in Figure 9b), the surface and interior has become

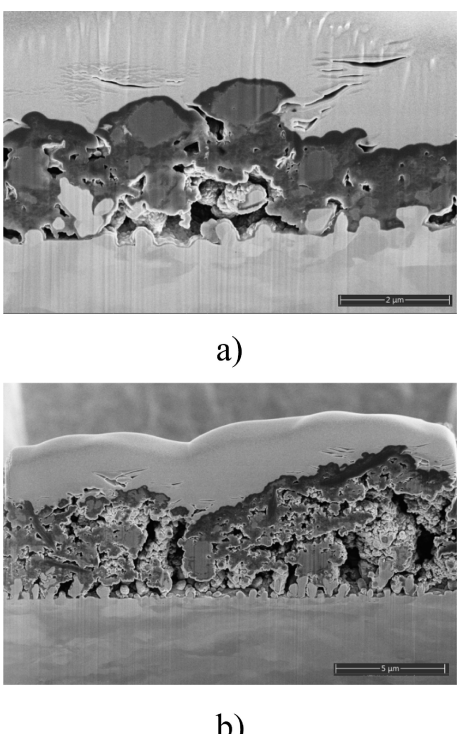


Figure 8. SEM micrographs of cross sections of Si electrodes after 10 cycles in full-cell configuration with NMC442 cathode with electrolytes of a) 1 M LiFSI b) 1 M LiPF₆.

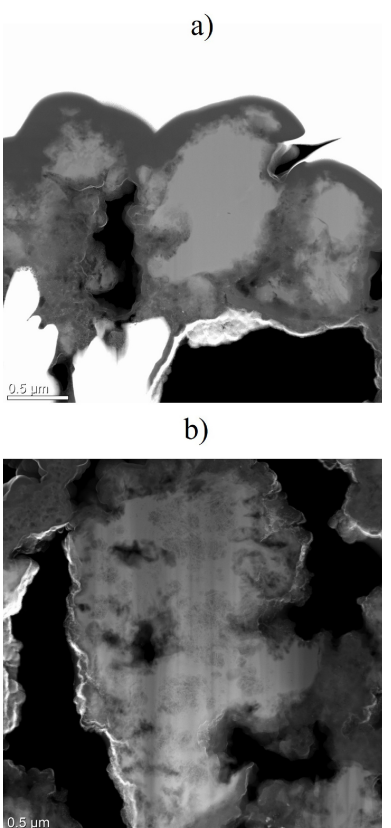


Figure 9. High angle annular dark field scanning transmission electron microscopy image of Si particles in Si electrodes cycled 10 times in full-cell configuration with NMC442 cathode with either a) 1 M LiFSI or b) 1 M LiPF₆ electrolyte.

highly roughened. The largest Si particle in Figure 9a) shows little sign of roughening, even though the capacity achieved with these cells actually were higher for the cell with LiFSI electrolyte. Hence, the nonuniform lithiation of the Si particles in LiPF₆ electrolyte must be due to less uniform SEI layer. More micrographs of Si particles from these electrodes are given in Supporting Information, Figure S8.

SEI Composition of Silicon Electrodes Cycled in Full Cells

TEM element analysis

Figure 10 show element analysis by TEM of the two Si electrodes discussed above. Figures 10a) and 10c) show the same sample region, but mapped for different elements, of the Si electrode cycled 10 times in 1 M LiFSI. Similarly, Figure 10b) and 10d) show the same sample region, but mapped for different elements, of the Si electrode cycled 10 times in 1 M LiPF₆. In Figures 10a) and 10b) red is silicon, green is carbon and blue is lithium. In Figures 10c) and 10f) red is lithium, green is fluorine and blue is oxygen, hence overlap between lithium and fluorine become yellow and overlap between lithium and oxygen become purple.

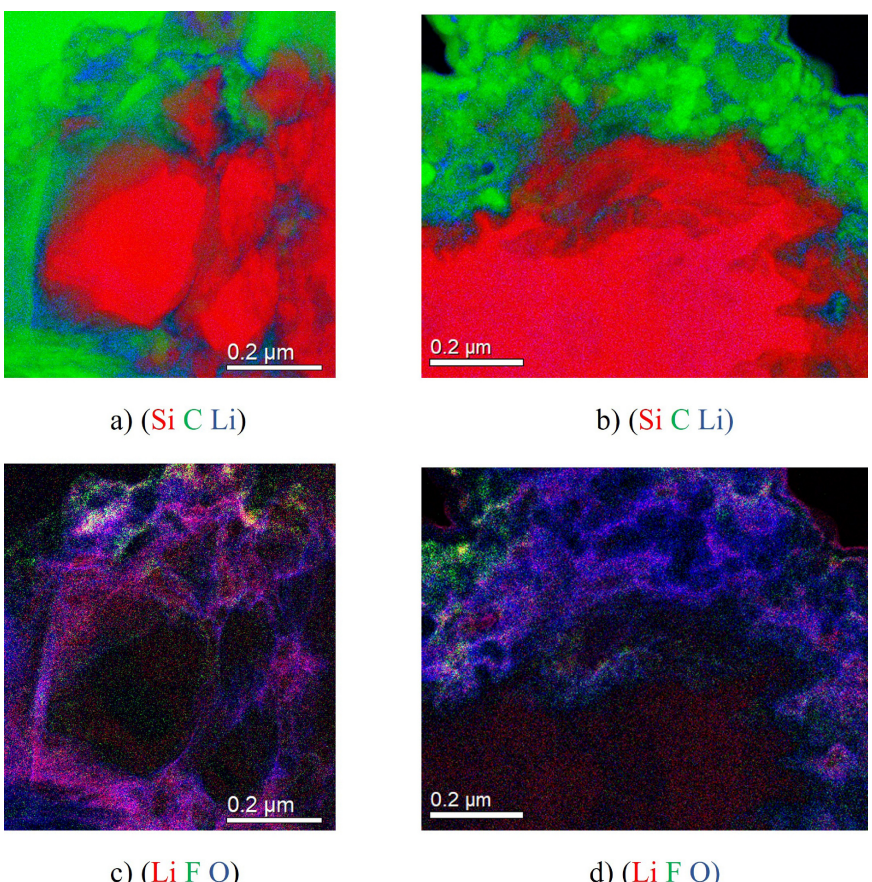


Figure 10. Combined and colored element maps acquired by TEM element analysis of Si electrodes cycled 10 times in full-cell configuration with NMC cathode with either 1 M LiFSI a) and c) or 1 M LiPF₆ b) and d) electrolyte.

After cycling in 1 M LiFSI electrolyte (Figures 10a) and 10c), lithium is primarily detected around the Si particles and there is a strong overlap between lithium and oxygen. Some overlap between lithium and fluorine is evidenced in the upper part of Figure 10c), where small Si particles are located. Also, some lithium is detected within the Si particles, especially near the particle edges.

After 10 cycles in 1 M LiPF₆ electrolyte, Figures 10b) and 10d), some differences are evident compared to after cycling in 1 M LiFSI electrolyte. Here, the detected amount of lithium within the silicon particle is quite high, while less is found in the particle surroundings. As the images are taken from cross sections of the particles after discharge, this indicates that more lithium is trapped after cycling in the 1 M LiPF₆ electrolyte compared to in 1 M LiFSI electrolyte. For both electrodes, the Si particle surroundings have a high concentration of oxygen, however the overlap between lithium and oxygen for the electrode cycled in LiPF₆ electrolyte is much less evident than for the electrode cycled in LiFSI electrolyte. Some overlap between lithium and fluorine is observed in the left and upper right part of Figure 10d), predominantly in between carbon black particles, and not close to silicon. This same feature, with LiF positioned in the SEI quite far from Si particles surrounding carbon black particles, was seen when cycling Si electrodes in half-cells with 1 M LiPF₆ electrolyte.^[14] In Figure 10, the LiF is

found as small grains though, while after cycling in half-cells, the LiF had assembled in larger clusters.

XPS

Table 2 shows the elemental composition, in atom%, of the surface of the Si electrodes cycled 10 or 50 times in full-cells with either 1 M LiFSI or 1 M LiPF₆ electrolyte. The surface analysis of a fresh, uncycled Si electrode is also included in the table. Trace amounts of Na, Cu and minor impurities are not included. The percentages of the different elements detected on the electrodes cycled in LiFSI electrolyte show very little variation with cycling, suggesting a very stable SEI. The salt reduces first in this electrolyte, and since only small variations in the percentages of the inorganic elements (F, Li, N and S) can be seen, we take this as an indication of a good, flexible and passivating SEI. For the electrodes cycled in LiPF₆ electrolyte on the other hand, the percentage of lithium and oxygen increased and percentage of carbon decreased with cycling, indicating a less stable SEI with cycling compared to in the LiFSI electrolyte. It should also be noted that the LiFSI electrodes have notably higher percentages of oxygen and lower percentages of fluorine and lithium compared to the LiPF₆ electrodes.

Table 2. Elemental composition in atom% of Si electrode surface before and after full-cell cycling against NMC cathode in either 1 M LiFSI or 1 M LiPF₆ electrolyte, acquired from survey spectra obtained with XPS.

Element	Si	O	C	F	Li	N	S	P
Fresh electrode	5.4	20.2	73.7	—	—	—	—	—
10th cyc 1 M LiFSI	—	43.3	29.2	10.9	12.8	1.3	1.2	—
50th cyc 1 M LiFSI	—	43.6	31.3	9.6	11.7	2.0	1.6	—
10th cyc 1 M LiPF ₆	—	31.6	32.0	16.8	17.2	—	—	1.0
50th cyc 1 M LiPF ₆	—	33.7	28.0	16.7	20.3	—	—	—

Figure 11 shows the C 1s spectra of the Si electrodes after 10 and 50 cycles in full-cell configuration in electrolyte containing either 1 M LiFSI, Figures 11a) and 11c), or 1 M LiPF₆, Figures 11a) and 11d). The peak with the lowest binding energy, at 282.8 eV, is assigned to lithiated carbon.^[64,68] The peak at 285 eV is assigned to C–C/C–H (adventitious carbon), the peak at 286.3 eV is assigned to C–O, and the peak at 290 eV is assigned to carbonates, CO₃.^[10,45,64–67,76–78] The peak at 288.7 eV is assigned to O=C=O/C=O.^[10,67,76,77] For the electrodes cycled 50 times, the peak at 291 eV is assigned to FEC reduction products.^[66,67]

The main difference observed from the C 1s spectra, is the significantly higher peak at 282.8 eV, Li_xC, after 10 cycles for LiPF₆. After 50 cycles, the percentages of Li_xC are almost equal for the two electrolytes. Also after 50 cycles, the percentage of carbonate has increased for both electrodes at the expense of the percentage of adventitious carbon, and a peak for the FEC reduction product have appeared in the spectra. This peak is larger for the electrode cycled in LiPF₆ electrolyte than the one cycled in LiFSI electrolyte, suggesting more FEC reduction due to SEI cracking during lithiation/delithiation. From the SEM and TEM micrographs, lithiation appears less uniform for the electrode cycled in LiPF₆ compared to the LiFSI electrolyte, hence more SEI damage and reformation is expected. In the LiPF₆ electrolyte, FEC has the highest reduction potential, thus FEC reduces first when SEI is formed in this electrolyte. Thus, detection of less FEC reduction product and stable percentages of inorganic elements on the Si electrode cycled in LiFSI electrolyte suggests less SEI damage.

Figure 11 shows the O 1s spectra for the Si electrodes cycled in LiFSI 10 and 50 times, Figures 11e) and 11f), and in LiPF₆ 10 and 50 times, Figures 11g) and 11 h). Dotted lines are included in the spectra at the binding energies for expected environments, namely C=O at 531.8 eV and C–O at 533.4 eV.^[64,66–68] The binding energy for Li₄SiO₄ at 530 eV^[78] is marked in the spectra, along with the binding energy for a reduction product of FEC at 534, here denoted poly(FEC).^[78] None of the spectra show a distinct shoulder in the peak at these energies. In general, the O1s spectra are difficult to resolve, and thus only provide information about the dominating bonds.

All the C 1s spectra show the peak centered around the binding energy of C=O. When evaluating the features in the spectra it must be considered that carbonates (Li₂CO₃) only contribute to the C=O feature of C1s, while organic compo-

nents contribute to both the C–O feature and the C=O feature.^[68] Therefore, organic components are very likely contributing to the C=O feature in the O 1s spectra here for all the samples.

In Table 1 it can also be seen that the ratio between lithium and fluorine was quite stable with cycling in LiFSI, while in LiPF₆ electrolyte an increase in amount of lithium with cycling increases the ratio. After 50 cycles the difference is more carbonate and FEC reduction product on the electrode cycled in LiPF₆ electrolyte. The F 1s and Li 1s spectra show no significant differences and are presented in Supporting Information, Figure S9.

Regarding the SEI formation, the benefits of the LiFSI electrolyte, as identified from half-cell experiments, are still recognized in the electrodes cycled in full cells. The SEI formed appears more flexible, as seen from the cross section micrographs, and with smaller amounts of FEC reduction products observed. From the TEM element map, the electrode cycled in LiPF₆ appears to have more trapped lithium, both in the silicon particles, and in the carbon, which is also consistent with the lower coulombic efficiency and the higher degradation rate for this electrolyte. Furthermore, the same tendency for clustering of LiF around carbon black particles is observed, although less pronounced than for the electrodes cycled in half cells. In LiFSI less lithium was detected in the Si particles and large amounts of lithium oxide in the surroundings. This suggests that the SEI from LiFSI consist of more species containing lithium and oxygen, like Li₂O and Li₂CO₃, than the SEI from LiPF₆. As previously shown,^[48] the lower surface area of the silicon used for these anodes is beneficial in terms the lower amount of SEI formation and repair during cycling.

Conclusions

LiFSI-based electrolytes, with LiBF₄ and LiDFOB as additives, have been investigated with the aim of demonstrating cycling in full cells with a cathode voltage >4.3 V. The performance of the electrolytes was first studied separately in high content silicon anodes (60 wt% micronsized Si, 10 wt% graphite), NMC442 cathodes, and the aluminium current collector, by electrochemical methods and post mortem analysis (SEM imaging and XPS). Electrolytes with LiDFOB as additive were shown to exhibit the lowest oxidation currents for aluminium current collectors, with almost no visible changes to the surface

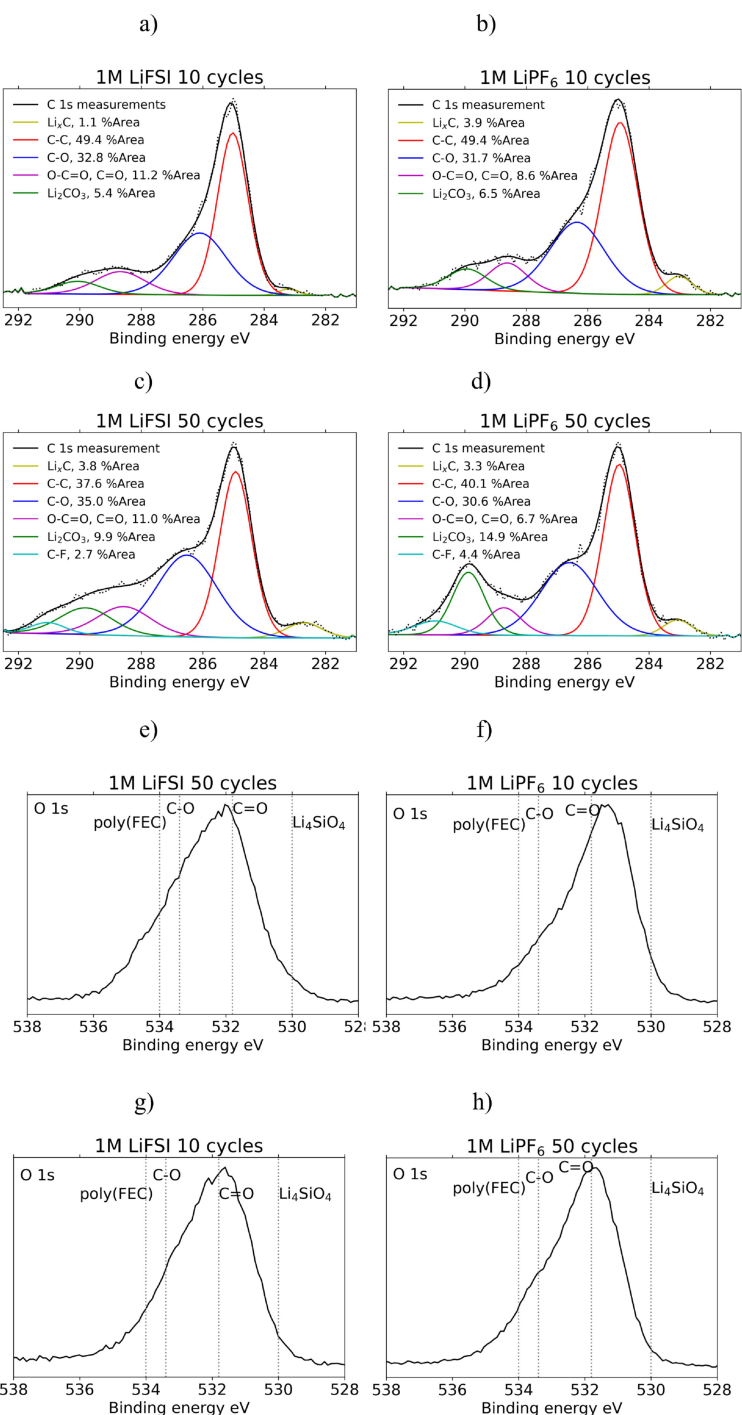


Figure 11. C 1s and O 1s spectra recorded for Si electrodes after cycling in full cells. a) C 1s spectra for Si electrodes cycled 10 times in 1M LiFSI b) C 1s spectra for Si electrodes cycled 50 times in 1M LiFSI c) C 1s spectra for Si electrodes cycled 10 times in 1M LiPF₆ d) C 1s spectra for Si electrodes cycled 50 times in 1M LiPF₆ e) O 1s spectra for Si electrodes cycled 10 times in 1M LiFSI f) O 1s spectra for Si electrodes cycled 50 times in 1M LiFSI g) O 1s spectra for Si electrodes cycled 10 times in 1M LiPF₆ h) O 1s spectra for Si electrodes cycled 50 times in 1M LiPF₆.

(from SEM micrographs), while the XPS spectra confirmed the presence of Al–O–F and Al–F features. Similarly, this electrolyte showed the best performance of silicon anodes in half cells, with an SEI rich in organic compounds, and less LiF. The addition of LiBF₄ also significantly reduced the oxidation currents for the aluminium current collector, and the surface was verified to be enriched in Al–F features (from XPS).

However, the silicon anodes showed an inferior performance in this electrolyte, with an SEI rich in LiF. Thus, for anodes with a high silicon content, the addition of a hydrolyzing salt appears to disrupt the good SEI forming properties of LiFSI. Upon cycling of NMC442 cathode in half cells with the same electrolytes, stable performance was observed for all, at a cut-off voltage of 4.2 V. At 4.5 V, rapid degradation was observed for

the LiFSI electrolyte, while the capacity was stable upon cycling in LiFSI with LiBF₄ or LiDFOB added. The good performance of the LiDFOB additive could also be verified in full cells, composed of silicon-graphite anodes (60 wt% Si) and NMC442. Thus, the combination of LiFSI and LiDFOB salts can significantly reduce the content of fluorine compared to conventional electrolytes based on LiPF₆.

Furthermore, it could be verified that the benefits of the LiFSI salt with respect to SEI formation on the silicon anode observed in half cells was also preserved in full cells. The XPS results indicated that the SEI formed in LiFSI electrolyte was more stable with cycling in full cells, than the SEI formed in the reference LiPF₆ electrolyte, and likely to be more flexible and conductive, as indicated from the more uniform lithiation of the silicon particles in the LiFSI electrolyte. While the SEI formed in the LiFSI electrolyte is rich in Li₂O and Li₂CO₃, the content of LiF is much higher for the SEI formed in LiPF₆, and located around the carbon black particles.

Experimental

Electrochemical characterization

Electrode preparation

Silicon electrodes were prepared by making a slurry of 60 wt% Si (Silgrain®, e-Si 400, a commercially available battery grade silicon from Elkem), with an average particle size of 3 µm, 10 wt% graphite (KS6 L, Imerys), 15 wt% carbon black (C-NERGY C65, Imerys) and 15 wt% Na-CMC binder (Sigma Aldrich Mw ≈ 90000). An aqueous buffer with citric acid and potassium hydroxide at pH = 3 was used as solvent. The slurry was cast onto dendritic copper foil and dried at 120 °C under vacuum.^[79]

Cathodes were made from a slurry containing 80 wt% NMC442 (BC-723 K, 3 M), 10 wt% carbon black (Timcal, C-NERGY C65) conductive additive and 10 wt% PVDF binder (polyvinylidene, Arkema). The slurry was homogenized in a radially oscillating mixer (RETSCH MM400) at 15 Hz for 45 minutes. The slurry was tape-casted onto Al foil (15 µm thickness, Hydro), by means of a coater (KR – K Control Coater), resulting in a wet-film thickness of ca. 150 µm. Electrodes were subsequently dried in a ventilated convection oven at 60 °C, and circular electrodes of 1.6 cm diameter were punched from the casts. The capacity of the cathodes were in the range ≈ 0.40–0.45 mAh cm⁻², with a thickness of ≈ 30 µm as determined by using a digital caliper. The electrodes were dried in vacuum at 120 °C and were finally kept in an Ar-filled glovebox (O₂ < 0.1 ppm, H₂O < 0.1 ppm) prior to cell assembly.

Half-cell characterization of silicon-graphite electrodes

For half-cell characterization, silicon electrodes were assembled in CR2016 coin cells (Hohsen) with Li metal as counter electrode and Celgard 2400 as separator. The electrolytes used were 1 M LiFSI (> 99.9%, American Elements), 1 M LiFSI + 0.2 M LiBF₄ (> 99.99% anhydrous, Sigma Aldrich) or 1 M LiFSI + 0.2 M LiDFOB (anhydrous, Sigma Aldrich) in EC, PC and diethyl carbonate (DEC) (1:1:3 by wt, anhydrous, Sigma Aldrich) with 1 wt% vinylene carbonate (VC) (97%, Sigma Aldrich) and 5 wt% FEC (> 99%, acid < 200 ppm, anhydrous, Sigma Aldrich). Cell assembly was done in an Ar-filled glovebox. The cells were cycled using a BioLogic BCS 805 battery

cycler. The cells underwent one formation cycle at C/20 before 100 cycles at C/2 in voltage range 0.05–1.0. The C-rate was defined as 1 C corresponding to 3600 mAh/g(Si).

Half-cell characterization of NMC electrodes and aluminium current collectors

For characterization of NMC half-cells, NMC electrodes were assembled in aluminum bags coated with polypropylene (pouch cells) with Li metal as counter electrode and Celgard 2400 as separator. Aluminium current collectors were characterized electrochemically in the same configuration. The electrolytes used were the same as for the silicon-graphite electrodes. Cell assembly was done in an Ar-filled glovebox. Electrochemical characterization was performed on a BioLogic BCS 805 battery cycler. The cells were subjected to one formation cycle at C/10 and 59 cycles at 1 C in voltage ranges 3.0–4.2 V and 3.0–4.5 V. 1 C was defined as 150 mAh/g(NMC).

Characterization of NMC-Silicon full cells

Silicon and NMC electrodes were assembled in pouch cells using aluminum bags coated with polypropylene. The NMC electrodes contained 6.1 +/− 0.2 mg NMC, amounting to 0.45 +/− 0.02 mAh cm⁻². This translates to a capacity of approximately 2000 on the silicon electrodes, where loading was 0.2 mAh cm⁻² silicon. Celgard 2400 was used as separator. The silicon and NMC electrodes were 16 mm in diameter. Cell assembly was done in an argon filled glove box. Electrolytes used were 1 M LiPF₆ (battery grade, Sigma Aldrich), 1 M LiFSI (> 99.9%, American Elements), 1 M LiFSI + 0.2 M LiDFOB, (anhydrous, Sigma Aldrich) in EC, PC and DEC (1:1:3 by wt, anhydrous, Sigma Aldrich) with 1 wt% VC (97%, Sigma Aldrich) and 5 wt% FEC (> 99%, acid < 200 ppm, anhydrous, Sigma Aldrich).

Galvanostatic cycling was performed using a BioLogic BCS 805 battery cycler. Experiments were performed at constant currents where C-rate was defined as 1 C = 150 mAh/g (NMC). Standard galvanostatic cycling was performed in the voltage range 2.2–4.3 V. The first cycle was done at C/10 and continued cycling at C/2. After each charge and discharge a constant voltage step was applied until the current decreased to C/4.

Post mortem characterization

For post mortem characterization of silicon electrodes, full-cells were cycled in pouch cells for 10 or 50 cycles (after the formation cycle). Thereafter, the cells were disassembled in an argon filled glove box, rinsed with DMC and dried under vacuum at 70 °C for 3 hours. The electrodes were further mounted on sample stubs and transferred to FIB and XPS.

Cross-section TEM samples were prepared with a Helios G4 UX focused ion beam (FIB). Carbon or Pt layers were first deposited on top of the electrode to protect the area of interest below. The first part of the protection layer was deposited by electron beam assisted deposition. Thick lamellas were cut out and transferred to dedicated Cu TEM half-grids by standard lift-out technique. Coarse thinning was performed with 30 kV ion-beam acceleration voltage. Final thinning was done at 5 and 2 kV on either side of the lamellas to minimize ion-beam induced surface damage. TEM was performed with a double Cs aberration corrected cold-FEG JEOL ARM 200CF, operated at 200 kV. The instrument is equipped with a 100 (0.98 sr solid angle) Centurio SDD for energy dispersive X-ray spectroscopy (EDS) and a Quantum ER GIF for dual electron energy loss spectroscopy (EELS). All spectroscopy was done in STEM-mode

and by performing EDS and dual-EELS simultaneously during mapping.

XPS characterization was performed by a Kratos Analytical Axis Ultra DLD XPS. The XPS uses an aluminum monochromatic X-ray source operating at 100 W. For each sample, three survey scans with pass energy 160 eV and resolution 0.5 eV from 1200–0 eV were performed in order to identify the elements present on the anode. Next, each core peak of interest underwent 3–7 narrow scans, depending on ease of detection, at pass energy 20 eV with resolution 0.1 eV or 0.05 eV in order to get high resolution data. The measurements were done at 1×10^{-9} , with an acceleration voltage of 12 kV and a 12 mA beam current. To avoid exposing the electrodes to air, an inert transfer arm was used when transferring the samples from the glove box to the XPS. The resulting data were processed using the software CasaXPS. The XPS spectra, both survey scan and all core peaks, were energy calibrated with respect to the adventitious carbon peak in the C 1s spectrum, which is positioned at binding energy 285 eV. A tough background was used when fitting the peaks.

Acknowledgements

The Research Council of Norway (RCN), as well as the industrial partners Elkem Technology AS and Dupont Nutrition and Health are acknowledged for the financial support of this work, within the KpN project "SiBEC" (contract no. 255195), through the ENERGIX program. RCN is also acknowledged for the support to the Norwegian Micro- and Nano-Fabrication Facility, NorFab (contract no. 245963), as well as for the support to the TEM work, carried out in the NORTEM infrastructure (contract no. 197405). Dr. Øystein Dahl, SINTEF Industry, is acknowledged for assistance with xps measurements.

Conflict of Interests

The authors declare no conflict of interest.

Data Availability Statement

The data that support the findings of this study are available from the corresponding author upon reasonable request.

Keywords: Li-ion · Silicon · LiFSI · LiDFOB

- [1] B. Scrosati, J. Garche, *J. Power Sources* **2010**, *195*, 2419.
- [2] D. Bresser, A. Moretti, A. Varzi, S. Passerini, in *Encyclopedia of Electrochemistry*, Wiley-VCH Verlag GmbH & Co. **2020**.
- [3] Y. Zhang, N. Du, D. Yang, *Nanoscale* **2019**, *11*, 19086.
- [4] W. F. Ren, Y. Zhou, J. T. Li, L. Huang, S. G. Sun, *Curr. Opin. Electrochem.* **2019**, *18*, 46.
- [5] H. Wu, Y. Cui, *Nano Today* **2012**, *7*, 414.
- [6] C. L. Campion, W. Li, B. L. Lucht, *J. Electrochem. Soc.* **2005**, *152*, 2327.
- [7] J. Vetter, P. Novak, M. R. Wagner, C. Veit, K. C. Moller, J. O. Besenhard, M. Winter, M. Wohlfahrt-Mehrens, C. Vogler, A. Hammouche, *J. Power Sources* **2005**, *147*, 269.
- [8] S. Lux, I. Lucas, E. Pollak, S. Passerini, M. Winter, R. Kostecki, *Electrochim. Commun.* **2012**, *14*, 47.
- [9] D. Aurbach, B. Markovsky, A. Rodkin, E. Levi, Y. S. Cohen, H. J. Kim, M. Schmidt, *Electrochim. Acta* **2002**, *47*, 4291.
- [10] B. Philippe, R. Dedryvvere, M. Gorgoi, H. Rensmo, D. Gonbeau, K. Edström, *J. Am. Chem. Soc.* **2013**, *135*, 9829.
- [11] Y. Cai, H. Zhang, Y. Cao, Q. Wang, B. Cao, Z. Zhou, F. Lv, W. Song, D. Duo, L. Yu, *J. Power Sources* **2022**, *535*, 231481.
- [12] Z. Du, D. L. Wood, I. Belharouak, *Electrochim. Commun.* **2019**, *103*, 109.
- [13] H. Shobukawa, J. Shin, J. Alvarado, C. S. Rustomji, Y. S. Meng, *J. Mater. Chem. A* **2016**, *4*, 173.
- [14] K. Asheim, P. Vullum, N. Wagner, H. Andersen, J. Mæhlen, A. Svensson, *RSC Adv.* **2022**, *12*, 12517.
- [15] Z. Chang, X. Li, F. Yun, Z. Chao, Z. Hui, J. Wang, S. Lu, *ChemElectroChem* **2020**, *7*, 1135.
- [16] G. G. Eshetu, T. Diemant, S. Grugeon, R. J. Behm, S. Laruelle, M. Armand, S. Passerini, *ACS Applied Materials and Interfaces* **2016**, *8*, 16087.
- [17] J. Kalhoff, G. G. Eshetu, D. Bresser, S. Passerini, *ChemSusChem* **2015**, *8*, 2154.
- [18] H. B. Han, S. S. Zhou, D. J. Zhang, S. W. Feng, L. F. Li, K. Liu, W. F. Feng, J. Nie, H. Li, X. J. Huang, M. Armand, Z. B. Zhou, *J. Power Sources* **2011**, *196*, 3623.
- [19] J. Zheng, J. A. Lochala, A. Kwok, Z. D. Deng, J. Xiao, *Adv. Sci.* **2017**, *4*, 1700032.
- [20] K. Matsumoto, K. Inoue, K. Nakahara, R. Yuge, T. Noguchi, K. Utsugi, *J. Power Sources* **2013**, *231*, 291.
- [21] T. Evans, J. Olson, V. Bhat, S. H. Lee, *J. Power Sources* **2014**, *269*, 616.
- [22] Q. Liu, T. L. Dzwiniel, K. Z. Pupek, Z. Zhang, *J. Electrochem. Soc.* **2019**, *166*, A3959.
- [23] I. A. Shkrob, K. Z. Pupek, D. P. Abraham, *J. Phys. Chem. C* **2016**, *120*, 18435.
- [24] P. Meister, X. Qi, R. Kloepsch, E. Kramer, B. Streipert, M. Winter, T. Placke, *ChemSusChem* **2017**, *10*, 804.
- [25] X. Zhang, T. Devine, *J. Electrochem. Soc.* **2006**, *153*, B375–B383.
- [26] T. Ma, G. Xu, Y. Li, L. Wang, X. He, J. Zheng, J. Liu, M. Engelhard, P. Zapol, L. Curtiss, J. Jorne, K. Amine, Z. Chen, *J. Phys. Chem. Lett.* **2017**, *8*, 1072.
- [27] S.-W. Song, T. J. Richardson, G. V. Zhuang, T. M. Devine, J. W. Evans, *Electrochim. Acta* **2004**, *49*, 1483.
- [28] A. Hofmann, M. Schulz, V. Winkler, T. Hanemann, *J. Electrochem. Soc.* **2014**, *161*, A431.
- [29] S. S. Zhang, *Electrochim. Commun.* **2006**, *8*, 1423.
- [30] K. Park, S. Yu, C. Lee, H. Lee, *J. Power Sources* **2015**, *296*, 197.
- [31] G. Yan, X. Li, Z. Wang, H. Guo, W. Peng, Q. Hu, *J. Solid State Electrochem.* **2016**, *20*, 507.
- [32] S. Zugmann, D. Moosbauer, M. Amereller, C. Schreiner, F. Wudy, R. Schmitz, R. Schmitz, P. Isken, C. Dippel, R. Muller, M. Kunze, A. Lex-Baldacci, M. Winter, H. J. Gores, *J. Power Sources* **2011**, *196*, 1417.
- [33] S. Dalavi, P. Guduru, B. L. Lucht, *Journal of the Electrochemical Society* **2012**, *159*, A642.
- [34] S. Lee, J. Han, Y. Lee, M. Jeong, W. Shin, M. Ue, N. Choi, *Electrochim. Acta* **2014**, *137*, 1.
- [35] Z. Cao, X. Zheng, Q. Qu, Y. Huang, H. Zheng, *Adv. Mater.* **2021**, *33*, 210378.
- [36] K. Zhang, Y. Tian, C. Wei, Y. An, J. Feng, *Appl. Surf. Sci.* **2021**, *553*, 149566.
- [37] J.-Q. Huang, X. Guo, J. Huang, H. Tan, X. Du, Y. Zhu, B. Zhang, *J. Power Sources* **2021**, *481*, 228916.
- [38] M. Fang, J. Chen, B. Chen, J. Wang, *J. Mater. Chem. A* **2022**, *10*, 19903.
- [39] C. J. Jafta, X. G. Sun, G. M. Veith, G. V. Jensen, S. M. Mahurin, M. P. Paranthaman, S. Dai, C. A. Bridges, *Energy Environ. Sci.* **2019**, *12*, 1866.
- [40] M. Nie, B. Lucht, *Journal of the Electrochemical Society* **2014**, *161*, A1001.
- [41] B. Aktekin, G. Hernandez, R. Younesi, D. Brandell, K. Edström, *ACS Appl. Energ. Mater.* **2022**, *5*, 585.
- [42] S. E. Trask, K. Z. Pupek, J. A. Gilbert, M. Klett, B. J. Polzin, A. N. Jansen, D. P. Abraham, *J. Electrochem. Soc.* **2016**, *163*, A345.
- [43] S. D. Beattie, M. J. Loveridge, M. J. Lain, S. Ferrari, B. J. Polzin, R. Bhagat, R. Dashwood, *J. Power Sources* **2016**, *302*, 426.
- [44] R. E. Ruther, K. A. Hays, S. J. An, J. Li, D. L. Wood, J. Nanda, *ACS Appl. Mater. Interfaces* **2018**, *10*, 18641.
- [45] N. Dupré, P. Moreau, E. De Vito, L. Quazuguel, M. Boniface, A. Bordes, C. Rudisch, P. Bayle-Guillemaud, D. Guyomard, *Chem. Mater.* **2016**, *28*, 2557.
- [46] X. Wang, E. Yasukawa, S. Mori, *Electrochim. Acta* **2000**, *45*, 2677–2684.
- [47] K. Mun, T. Yim, C. Choi, R. Ryu, Y. Kim, S. Oh, *Electrochim. Solid-State Lett.* **2011**, *13*, A109.
- [48] N. P. Wagner, K. Asheim, F. Vullum-Bruer, A. M. Svensson, *J. Power Sources* **2019**, *437*, 226884.

- [49] Q. Dong, F. Guo, Z. Cheng, Y. Mao, R. Huang, F. Li, H. Dong, Q. Zhang, W. Li, H. Chen, Z. Luo, Y. Shen, X. Wu, L. Chen, *ACS Appl. Energ. Mater.* **2020**, *3*, 695.
- [50] H. Gao, F. Maglia, P. Lamp, K. Amine, C. Zonghai, *ASC Appl. Mater. Interfaces* **2017**, *9*, 44542.
- [51] M. Fu, K. Huang, S. Liu, J. Liu, Y. Li, *J. Power Sources* **2010**, *195*, 862–866.
- [52] X. Bian, S. Ge, Q. Pang, K. Zhu, Y. Wei, B. Zhou, F. Du, D. Zhang, *Journal of Alloys and Compounds* **2018**, *736*, 136.
- [53] Y. Zhu, Y. Li, M. Bettge, D. Abraham, *J. Electrochem. Soc.* **2012**, *159*, A2109.
- [54] X. Li, J. Zheng, M. Engelhard, M. Donghai, Q. Li, S. Jiao, N. Liu, W. Zhao, J.-H. Zhang, W. Xu, *ASC Appl. Mater. Interfaces* **2018**, *10*, 2469.
- [55] T. Yoon, N. Chapman, D. M. Seo, B. L. Lucht, *J. Electrochem. Soc.* **2017**, *164*, A2082.
- [56] S. Huang, S. Wang, G. Hu, L. Z. Cheong, C. Shen, *Appl. Surf. Sci.* **2018**, *441*, 265.
- [57] J. Alvarado, M. Schroeder, M. Zhang, O. Borodin, E. Gobrogue, M. Olguin, M. Ding, M. Gobet, S. Greenbaum, Y. Meng, K. Xu, *Mater. Today* **2018**, *21*, 341.
- [58] C. Jafta, X. Sun, H. Lyu, H. Chen, B. Thapaliya, W. Heller, M. Cuneo, R. Mayes, M. Paranthaman, S. Dai, C. Bridges, *Adv. Funct. Mater.* **2021**, *31*, 2008708.
- [59] D. Rogstad, M. Einarsrud, A. Svensson, *J. Electrochem. Soc.* **2021**, *168*, 110506.
- [60] B. S. Parimalam, B. L. Lucht, *Journal of The Electrochemical Society* **2018**, *165*, A251.
- [61] A. Xiao, L. Yang, B. L. Lucht, S.-H. Kang, D. P. Abraham, *J. Electrochem. Soc.* **2009**, *156*, A318.
- [62] M. Nie, D. P. Abraham, Y. Chen, A. Bose, B. L. Lucht, *J. Phys. Chem. C* **2013**, *117*, 1257.
- [63] K. Xu, *Chem. Rev.* **2014**, *114*, 11503.
- [64] C. Xu, F. Lindgren, B. Philippe, M. Gorgoi, F. Björefors, K. Edström, T. Gustafsson, *Chem. Mater.* **2015**, *27*, 2591.
- [65] G. M. Veith, M. Doucet, R. L. Sacci, B. Vacaliuc, J. K. Baldwin, J. F. Browning, *Sci. Rep.* **2017**, *7*, 6326.
- [66] F. Lindgren, C. Xu, L. Niedzicki, M. Marcinek, T. Gustafsson, F. Björefors, K. Edström, R. Younesi, *ACS Appl. Mater. Interfaces* **2016**, *8*, 15758.
- [67] A. L. Michan, B. S. Parimalam, M. Leskes, R. N. Kerber, T. Yoon, C. P. Grey, B. L. Lucht, *Chem. Mater.* **2016**, *28*, 8149.
- [68] K. Ciosek Höglström, S. Malmgren, M. Hahlin, H. Rensmo, F. Thebault, P. Johansson, K. Edström, *J. Phys. Chem. C* **2013**, *117*, 23476.
- [69] S.-J. Kang, K. Park, S.-H. Park, H. Lee, *Electrochim. Acta* **2018**, *259*, 949.
- [70] Y. Aoki, O. Mami, K. Sachiko, T. I. Yu, Y. N. Tsuyoshi, D. Takayuki, M. Inaba, *J. Phys. Chem. C* **2022**, *127*, 69.
- [71] B. Parimalam, B. Lucht, *Journal of The Electrochemical Society* **2018**, *165*, A251.
- [72] A. Andersson, M. Herstedt, A. Bishop, K. Edström, *Electrochim. Acta* **2002**, *47*, 1885.
- [73] N. Ehteshamia, A. Eguia-Barriob, I. Meatzab, W. Porcherc, E. Paillard, *J. Power Sources* **2018**, *397*, 52.
- [74] A. Abouimrane, J. Ding, I. J. Davidson, *J. Power Sources* **2009**, *189*, 186.
- [75] X. Wu, Z. Du, *Electrochim. Commun.* **2021**, *129*, 107088.
- [76] B. Philippe, R. Dedryvère, J. Allouche, F. Lindgren, M. Gorgoi, H. Rensmo, D. Gonbeau, K. Edströmm, *Chem. Mater.* **2012**, *24*, 1107.
- [77] B. Philippe, R. Dedryvère, M. Gorgoi, H. Rensmo, D. Gonbeau, K. Edström, *Chem. Mater.* **2013**, *25*, 394.
- [78] B. T. Young, D. R. Heskett, C. C. Nguyen, M. Nie, J. C. Woicik, B. L. Lucht, *ACS Appl. Mater. Interfaces* **2015**, *7*, 20004.
- [79] H. Andersen, C. Foss, J. Voje, R. Tronstad, T. Mokkelbost, P. Vullum, A. Ulvestad, M. Kirkengen, J. Mæhlen, *Sci. Rep.* **2019**, *9*, 14814.

Manuscript received: November 22, 2023

Revised manuscript received: February 13, 2024

Accepted manuscript online: February 14, 2024

Version of record online: March 6, 2024